J. Chem. Sci. (2021)133:41
https://doi.org/10.1007/s12039-021-01903-8

REGULAR ARTICLE

Visible light-induced catalytic abatement of 4-nitrophenol and Rhodamine B using ZnO/g-C_3N_4 catalyst

K V ASHOK KUMAR[a], T VINODKUMAR[a], M SELVARAJ[c], D SURYAKALA[b] and CH SUBRAHMANYAM[a,*]

[a]Department of Chemistry, Indian Institute of Technology, Hyderabad, Kandi 502285, India
[b]Department of Chemistry, GITAM University, Visakhapatnam 530045, India
[c]Department of Chemistry, Faculty of Science, King Khalid University, Abha 61413, Saudi Arabia
E-mail: csubbu@iith.ac.in

MS received 29 October 2019; revised 10 February 2021; accepted 2 March 2021

Abstract. In this study, pure ZnO and g-C_3N_4 were synthesized using coprecipitation and simple calcination methods, respectively. Further, ZnO is impregnated on a g-C_3N_4 surface with 10, 20 & 30 weight percentages, respectively. Besides, these materials are characterized by various physicochemical techniques such as PXRD, UV-Vis-DRS, TEM, PL, and FT-IR, etc. Vitally, as-prepared materials, catalytic activity was tested for removal of Rhodamine B and 4-nitrophenol from the wastewater under visible light irradiation. Among all these catalysts, 20 wt% ZnO/*g*-C_3N_4 showed better activity and showed 67% and 75% mineralization.

Keywords. ZnO/*g*-C_3N_4; 4-nitrophenol; Rhodamine B; Abatement; Mineralization.

1. Introduction

For a couple of decades, organic dyes and aromatic nitro compounds are being discharged into ecological water from various chemical industries such as printing, leather, textiles, plastic, cosmetics, pharmaceutical industries, etc., which has gotten primary worldwide attention due to their potential toxicity, mutagenic, teratogenic and cancer-causing properties, raising ecological concerns.[1,2] Consequently, the effective removal of these pollutants/contaminants from wastewater is a critical task.

To remove these pollutants, such as 4-nitrophenol and Rhodamine B, different techniques have been developed, such as oxidation,[3] reverse osmosis,[4] biological filtrations,[5] ion exchanges,[6] chemical precipitations,[7] adsorption[8], etc. However, alternatively, photocatalysis is the inexpensive and most accessible method to remove pollutants like phenol, p-cresol, and heavy metals from aqueous streams.[9–11] Due to the high quantum efficiency, non-toxicity, and low cost of ZnO, it has been considered for photocatalytic removal of pollutants.[12,13] As per the literature survey, Asher *et al.*, synthesized ZnO flowers for removal of surfactant nonylphenol ethoxylate degradation, Khan *et al.,* prepared ZnO nanoglobules for removal of Methyl orange, and Nagaraja *et al.,* developed ZnO nanopowder for removal of Rhodamine B under UV light irradiation. Zhang *et al.,* synthesized the ZnO spheres and photocatalytic activity was tested for removal of 4-Nitrophenol and Rhodamine B and Rajamanickam *et al.,* synthesized the ZnO nanoparticles for the removal of 4-Nitrophenol under solar light.[14–18] The pure ZnO has a wide bandgap (3.3 eV), and it shows excellent activity for organic pollutant degradation in aqueous suspension under an ultra-violet region.[19–22] Gratifyingly, the activity of photocatalyst (ZnO) increased by decreasing the bandgap of ZnO using doping with transition metals (Co, Mn, Fe, and Cu, etc.) and non-metals/carbonaceous materials (*g*-C_3N_4, GO, rGO, CNT's and CNF, etc.). From previous reports, g-C_3N_4 exhibited excellent photocatalytic activity. Notably, recent reports reveal that *g*-

*For correspondence

Supplementary Information: The online version contains supplementary material available at https://doi.org/10.1007/s12039-021-01903-8.

Published online: 10 April 2021

C_3N_4 displays tremendous photocatalytic activity in visible light, i.e., water splitting, CO_2 and NO_x reduction, removal of organic pollutants, etc.[23–32] Nonetheless, the fundamental disadvantage of g-C_3N_4 is quick electron-hole recombination and poor charge transport. This way, ZnO combined with g-C_3N_4 (ZnO/g-C_3N_4) could yield an excellent heterostructure to improve charge separation due to suitable band alignment.[33,34] In the recent past, Uma *et al.,* Chidambaram *et al.,* Chen *et al.,* Liang *et al.*, and Ji *et al.,* reported that ZnO/g-C_3N_4 showed excellent photocatalytic activity under visible light for removal of organic dyes.[35–39]

In addition to that, Kumar *et al.,* prepared N-doped ZnO/g-C_3N_4 composite by ultrasonic dispersion method, and photocatalytic activity was tested for removal of Rhodamine B from aqueous streams.[40] In this manuscript we focus on the removal of multiple pollutants (4-nitrophenol and Rhodamine B) with different weight ratios of ZnO and g-C_3N_4. We also optimize the effect of catalyst amount and concentrations of pollutant.

The highest percentages of removal and mineralization were observed for 4-nitrophenol and Rhodamine B. These are all major points to earlier reported work by Kumar *et al.,* ZnO and N-doped ZnO is used to trap the photoelectron from CB of g-C_3N_4 and suppress the recombination of electron-hole pairs and enhances the visible light activity in g-C_3N_4.

In this context, we synthesized the pure ZnO, g-C_3N_4, and ZnO/g-C_3N_4 with various weight percentages of ZnO *via* co-precipitation and deposition methods, respectively. These photocatalysts have been characterized by various physical-chemical techniques. Vitally, the photocatalytic activity of these materials was examined for the abatement of 4-Nitrophenol and Rhodamine B from wastewater. Also, kinetic studies and the effect of pollutants and catalytic concentrations were examined.

2. Experimental

2.1 *Chemicals used*

Zinc nitrate hexahydrate ($Zn(NO_3)_2{\cdot}6\ H_2O$) (Merck), Melamine (Alfa Aesar), 4-Nitrophenol (Sigma Aldrich), Rhodamine B (Sigma Aldrich), and Methanol (Fisher Scientific) were used without any further purification. Deionized water was used during the experiment.

2.2 *Synthesis of photocatalysts*

2.2.1. *Synthesis of pure ZnO* The pure ZnO was prepared by a simple co-precipitation method. Typically, 1 g of $Zn(NO_3)_2{\cdot}6\ H_2O$ was dissolved in 40 mL DI water. The resultant mixture was stirred on a hot plate for 15 min. Further, we added 10% NH_4OH solution dropwise, to reach pH $\sim$ 9. For extension, the stirring was continued for 3 h. After 3 h, the formed precipitate was recovered by centrifugation. The final material was washed with DI water and ethanol several times and kept in a hot air oven overnight drying at 80 °C. The dried material was calcined at 450 °C and used for further examinations and denoted as ZnO (**1**).

2.2.2. *Synthesis of pure g-C_3N_4* For the synthesis of g-C_3N_4, 10 g melamine was calcined in an alumina crucible at 550 °C for 4 h in the nitrogen gas atmosphere. The resulting material was used for further analysis, and it was named CN. (**2**).

2.2.3. *Synthesis of pure ZnO/g-C_3N_4* To synthesize the ZnO/g-C_3N_4 catalyst with different weight percentages of ZnO (10, 20 and 30 wt%), initially, we took the required amount of ZnO (10, 20 and 30 wt%) and g-C_3N_4 in the mortar mixed well and grained for 30 min. The resultant material was taken into the 10 mL of methanol, and the formed suspension was heated until complete methanol evaporation. Finally, the dried material was pelletized and calcined at 300 °C for 3 h. As developed, catalysts were denoted as 10 ZnO/CN (**3**), 20 ZnO/CN (**4**), and 30 ZnO/CN (**5**), respectively.

2.3 *Characterization*

The PANalytical X'pert Pro Powder X-ray diffractometer with Cu-Kα radiation, with a wavelength λ=1.54 Å and with a Ni filter is used for the phase quantification and crystal structure determination of all synthesized catalysts. UV-visible diffuse reflectance spectra of the samples were collected on Shimadzu-3600, with $BaSO_4$ as a standard reference. The particle size and morphology of the samples were recorded by Transmission electron microscopy (JEM-2100). The TEM images were recorded by inserting the sample onto a carbon-coated copper grid with an operating voltage of 200 kV. Samples from the Fourier transformation infrared spectrum (1-5) were measured using a Bruker ALPHA-E instrument with a resolution of 4 cm^{-1}. Photoluminescent properties of selected photocatalysts were recorded by Fluoromax-4-Spectrofluorometer (HORRIBA Scientific). The SHIMADZU TOC analyser confirmed the mineralization of pollutants (4-NP & RhB). The surface area of selected samples was analysed by Nova 2200e at

liquid nitrogen temperature. The surface area of catalyst ZnO is 26 m^2 g^{-1}, and the surface area of catalyst 20 ZnO/CN is ~50 m^2 g^{-1}.

2.4 *Photocatalytic activity test*

The photocatalytic activity of the catalysts (**1-5**) was carried out in the specially designed photocatalytic reactor, which consists of two (250 W) low voltage (24 V) non-halogen lamps with a light intensity of 500 to 550 W/m^2. The visible light activity of synthesized catalysts was tested for the removal of Rhodamine B and 4-Nitrophenol. In this typical experiment, we took 50 mg/50 mL of the catalyst in a round bottom flask and dispersed it in the aqueous solution pollutants, and kept it in the dark for 30 min to attain the adsorption-desorption equilibrium between pollutant and catalyst. It is worth mentioning that no conversion was observed either in the absence of the catalyst or light. After that, every 30 min, the mixture was collected and analysed by the UV-Vis spectrophotometer. The degradation of 4-Nitrophenol and Rhodamine B was monitored at wavelength 317 and 554 nm, respectively. The percentage of degradation of the pollutants was calculated by the formula shown in eq. 1:

$$\eta = \frac{C_0 - C_t}{C_0} \times 100 \quad (1)$$

where C_0 is the original concentration of a pollutant at time t=0, C_t is the final concentration of pollutants at time t, η is the pollutant degradation efficiency.[41–43]

TOC analysis was conducted to read the mineralization of 4-nitrophenol and Rhodamine B. Total organic carbon was measured with a TOC analyser (TOC-VCSH; SHIMADZU, Japan). The decrease in the percentage of TOC in pollutants was measured by the eq. 2:

$$\% \text{ of the decrease in TOC} = \frac{TOC_i - TOC_f}{TOC_i} \times 100 \quad (2)$$

Here, TOC_i is the initial value of TOC before the experiment and TOC_f is the final TOC value after 180 min visible light irradiation. The mineralization of 4-nitrophenol and Rhodamine B was investigated by monitoring the loss of TOC in the pollution solution.

3. Results and Discussions

3.1 *Powder-XRD analysis*

The crystalline properties and phase identification of (**1-5**) materials are displayed in Figure 1. The peak at 2θ value 27.7° with a lattice plane (002) confirms the presence of *g*-C_3N_4. The sharp peaks at d-spacing values of 2.819, 2.596, 2.478, 1.915, 1.624, 1.477 and 1.376 Å corresponds to (100), (002), (101), (102), (110), (103), and (112) planes of ZnO hexagonal wurtzite phase (JC-PDS number 36-1451). In the ZnO/CN catalyst, the crystalline phase of ZnO remains unchanged even after the g-C_3N_4 material has been impregnated. This phenomenon indicates the formation of a two-phase composite. The diffraction peaks of ZnO in ZnO/CN are slightly shifted to a higher angle than pure ZnO, indicating a good interaction between ZnO and g-C_3N_4 in the composite.[44–46]

3.2 *UV-VIS-DRS analysis*

The UV-Vis-DRS analysis of synthesized materials (**1-5**) is shown in Figure 2, which indicates that ZnO has

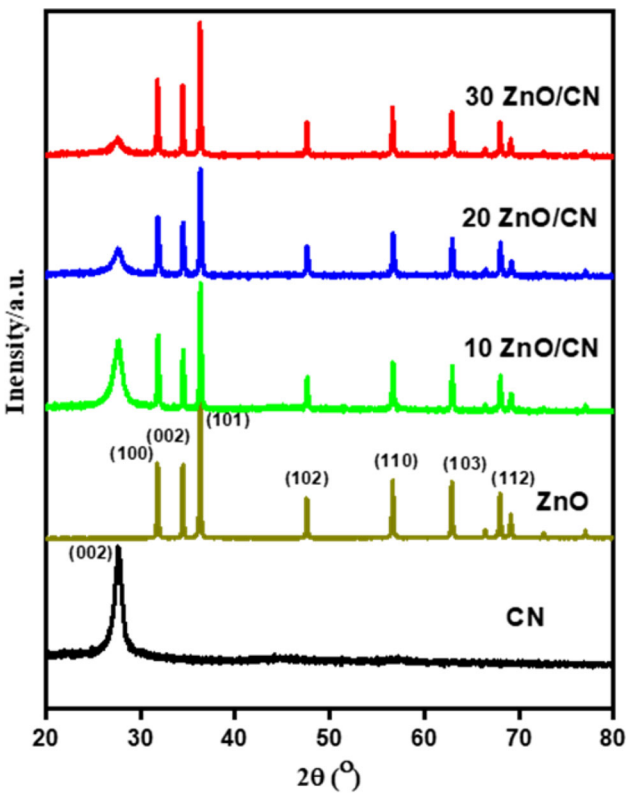

Figure 1. Powder-XRD patterns of **1-5** catalysts.

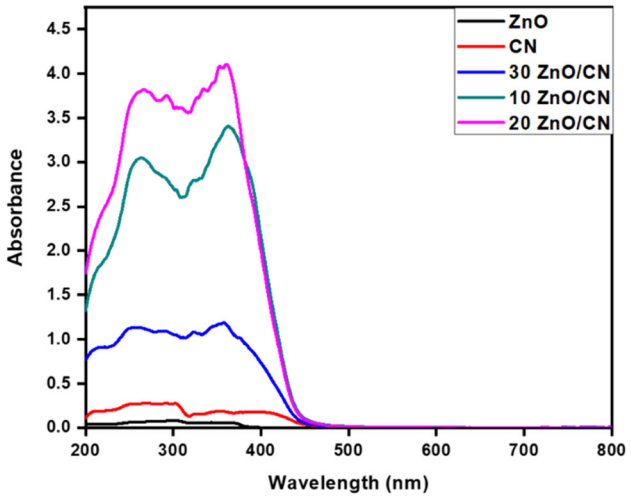

Figure 2. UV-Visible spectrum of **1**-**5** catalysts.

an absorption edge at 403 nm with a corresponding bandgap of 3.07 eV. Similarly, for g-C_3N_4, 30 ZnO/CN, 10 ZnO/CN, and 20 ZnO/CN composites show the band gap values at 2.7 eV, 2.37 eV, 2.33 eV, and 2.29 eV, respectively. Moreover, the absorption edges of ZnO/CN nanocomposites move towards the long wavelengths compared with pure ZnO, which reveals that the absorption edge of ZnO/CN photocatalyst moves to the lower energy region (visible region). These results imply that the visible light response of the photocatalysts has improved, and leads to a possible charge transfer between g-C_3N_4 and ZnO.[44] The formation of chemically bonded interfaces between ZnO and g-C_3N_4 makes the interparticle charge transfer process more spatially available and smoother, which is significant to enhance the photocatalytic activity.[47] The catalyst 20 ZnO/CN has the lowest bandgap of E_g=2.29 eV and the highest visible light activity compared to the remaining catalysts.[48,49]

3.3 *TEM analysis*

The TEM images of ZnO (**1**) and 20 ZnO/CN (**4**) are shown in Figure 3. The morphology of ZnO is hexagonal plate type structures, which are highlighted in Figure 3a. In Figure 3a, the inserted image represents the lattice fringes of ZnO a crystal plane (101) and an interplanar distance of 0.24 nm, which consistent with XRD observations. In Figure 3b, the ZnO nanoplates are randomly distributed on a surface of g-C_3N_4 sheets. From the TEM analysis, we conclude that there is a formation of heterojunction between g-C_3N_4 and ZnO.[50]

3.4 *Photoluminescence (PL) spectroscopy analysis*

The PL spectra of ZnO (**1**), g-C_3N_4 (**2**), and 20 ZnO/CN (**4**) are shown in Figure 4. Pure ZnO shows a broad emission peak at 464 nm, which is originated from oxygen and zinc intrinsic defects. Similarly, pure g-C_3N_4 shows a broad peak at 500 nm, which is subsequently suppressed in the ZnO/CN composite. In the ZnO/g-C_3N_4 composite, the intensity of the broad peak at 464 nm was reduced and slightly shifted to a higher wavelength which confirms the shifts in the bandgap towards the visible region. However, the PL intensity in ZnO/CN decreases due to a decrease in the charge recombination rate, which indicates the effective charge carrier separation capacity.[51] This shows that 20 ZnO/CN nanocomposite effectively conducts the photoexcited electrons to form superoxide radicals thereby enhancing the photocatalytic activity.[48,52,53]

3.5 *FTIR analysis*

The FTIR spectra of (**1-5**) photocatalysts are shown in Figure 5. In *g*-C_3N_4, the two broad peaks recognized at 1209 cm^{-1} and 1626 cm^{-1} are related to C-N and C=N stretching bands, and the peak at 800 cm^{-1} correspond to triazine units present in graphitic carbon nitride. In ZnO, the peaks between 679-1031 cm^{-1} represent the Zn-O stretching band, and peaks at 1374 cm^{-1} and 1597 cm^{-1} are associated with bending vibrations of hydroxyl residues which is due to atmospheric moisture.[54] Similar peaks of ZnO and g-C_3N_4 are observed in all composites indicate the formation of the ZnO/CN composite. The other important observation made from FTIR spectra was the structural features of g-C_3N_4 maintained in all composites. The ZnO/CN (3-5) peaks (1200 to 1800 cm^{-1}) slightly shifted to the higher wavenumber side compared to pure g-C_3N_4, (Figure 5) and this blue shift indicates the interaction between *g*-C_3N_4 and ZnO in composite (ZnO/CN).[44,55,56]

3.6 *Photocatalytic activity studies*

3.6a *Photocatalytic removal of Rhodamine B and 4-nitrophenol*: The visible light activity of prepared catalysts (1-5) was verified by the removal of individual pollutants 4-Nitrophenol (NP) and Rhodamine B (RhB). In the experiment, we observed that these pollutants (4-NP and RhB) degrade into non-toxic products (CO_2 and H_2O) under visible light irradiation. All pseudo-first-order rate constants are

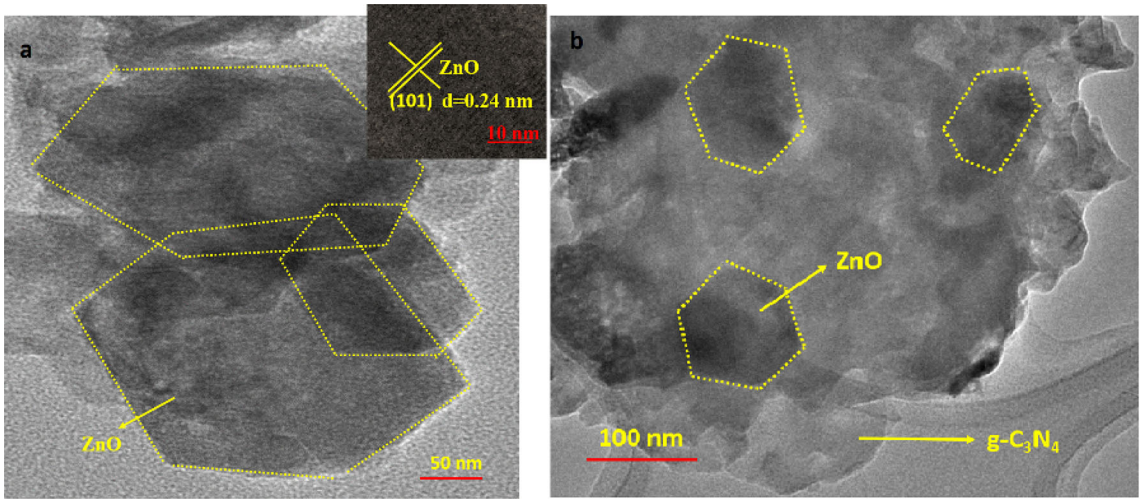

Figure 3. TEM image of (a) ZnO (**1**) (Lattice fringes of ZnO); (b) ZnO/CN composite (**4**).

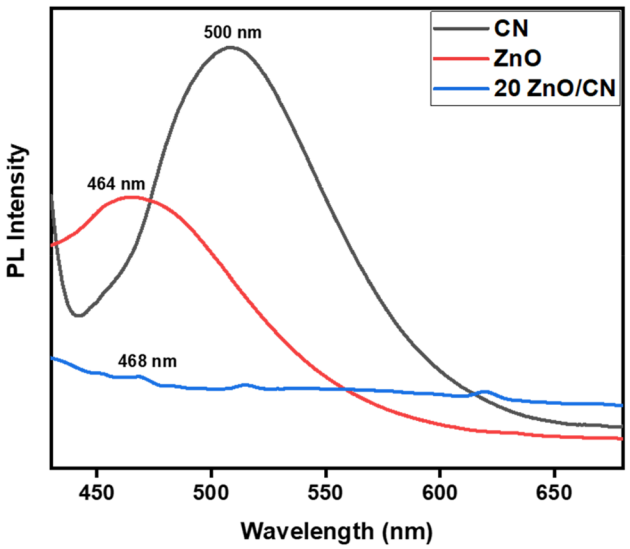

Figure 4. PL Spectra of ZnO (**1**), g-C_3N_4 (**2**), and ZnO/CN composite (**4**).

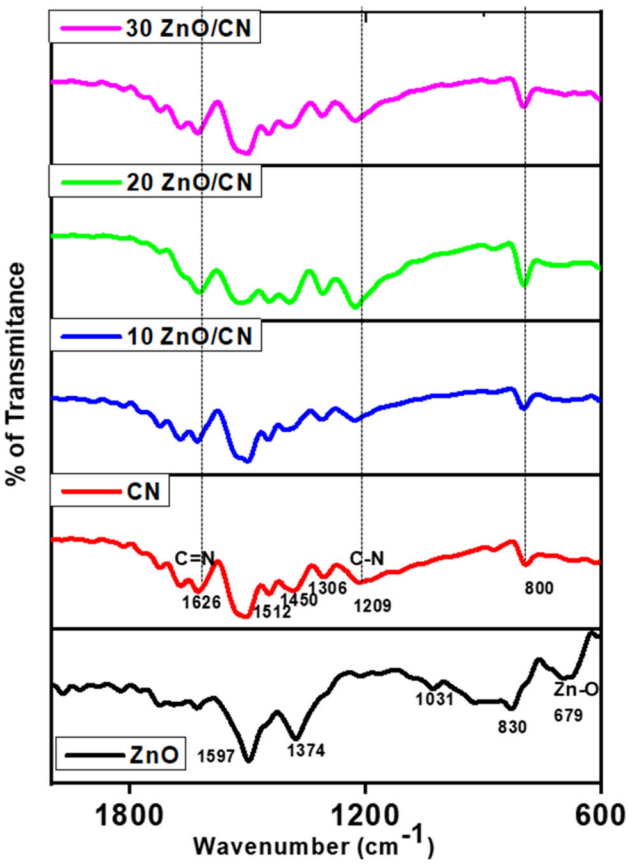

Figure 5. FTIR spectra of **1-5** catalysts.

calculated from the slope of the linearly fitted plots. From Figure 6a, the pseudo-first-order rate constant for (**1-5**) is found to be 2.69×10^{-3}, 2.85×10^{-3}, 3.09×10^{-3}, 5.72×10^{-3} and 4.73×10^{-3} min^{-1}, respectively. The photocatalyst 20 ZnO/CN shows the highest activity for 4-Nitrophenol when compare with other catalysts (**1**, **2**, **3** and **5**). From Figure 6b, the pseudo-first-order rate constant for Rhodamine B was found to be 2.58×10^{-3}, 4.02×10^{-3}, 4.49×10^{-3}, 7.49×10^{-3}, and 5.66×10^{-3} min^{-1}, respectively, for (**1-5**) materials. Based on the above results, we confirm the catalyst 20 ZnO/CN showed better photocatalytic activity. We found the degradation efficiency for 4-nitrophenol is 38%, 41%, 57%, 60%, 43% and the Rhodamine B showed 37%, 52%, 68%, 73% and 55%, respectively (Figure S1 in Suupplementary Information).

The decrease in percentages of TOC is measured for 4-nitrophenol and Rhodamine B and the results are presented in Table 1. The percentage of mineralization of 4-nitrophenol was 42%, 44%, 62%, 67% and 46%,

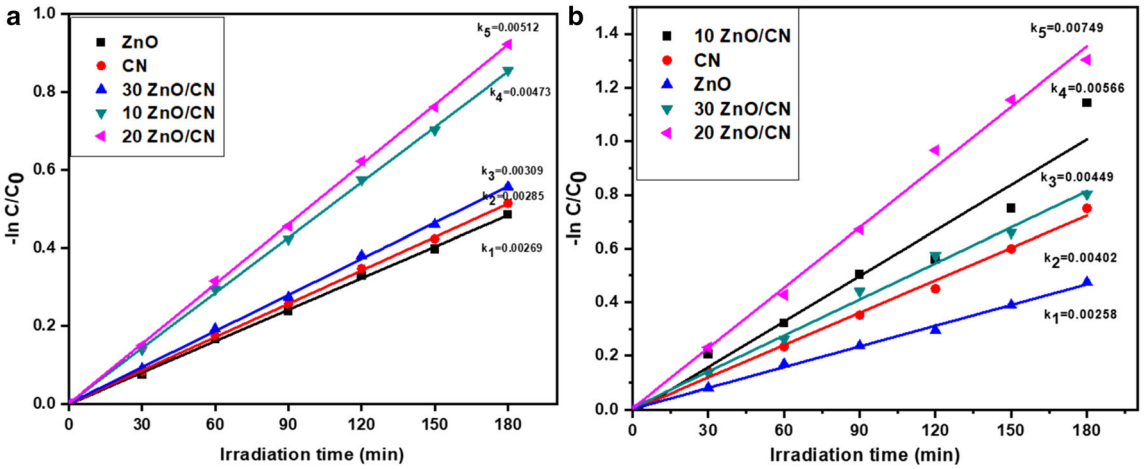

Figure 6. The kinetic plots for the pseudo-first-order reaction of (**a**) 4-Nitrophenol; (**b**) Rhodamine B (50 mg/50 mL catalysts, 10 ppm 4-NP, 10 ppm RhB, 3 h irradiation time).

Table 1. The decrease in TOC percentages of Rhodamine B and 4-nitrophenol.

Entry	Catalyst	4-nitrophenol (% in the decrease of TOC)	Rhodamine B (% in the decrease of TOC)
1	ZnO	58	56
2	CN	56	43
3	10 ZnO/CN	37	29
4	20 ZnO/CN	33	25
5	30 ZnO/CN	54	39

respectively. Whereas, Rhodamine B mineralization percentage was 44%, 57%, 71%, 75% and 61%, respectively. The results are displayed in Figure 7.

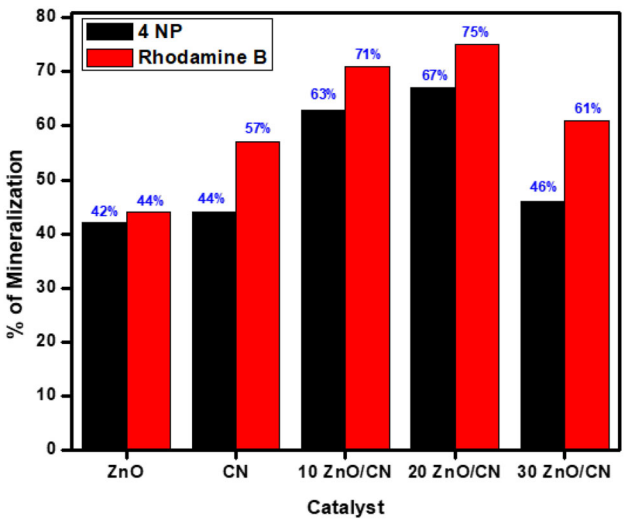

Figure 7. Catalytic mineralization of Rhodamine B and 4-Nitrophenol.

3.6b *Effect of concentration on the removal of Rhodamine B and 4-nitrophenol*: The effect of concentration plays a major role in the abatement of Rhodamine B and 4-nitrophenol. In this experiment, the concentration of both pollutants (4-NP & RhB) varied between 5 to 20 mgL^{-1}. As shown in Figure 8, the pseudo-first-order rate constant increased up to 10 mgL^{-1} (4.10×10^{-3}, 5.12×10^{-3} min^{-1} for 4-NP and 6.42×10^{-3}, 7.49×10^{-3} min^{-1} for RhB) and decreased for higher concentration (1.98×10^{-3} and 1.79×10^{-3} min^{-1} for 15 mgL^{-1} and 20 mgL^{-1} for 4-NP whereas, its rate constants for the same concentration was 3.67×10^{-3}, 1.79×10^{-3} min^{-1} for RhB). The decrement of catalyst activity at a higher concentration of pollutants is due to the higher quantity of molecules present on the catalyst surface, and these molecules partially prevent light absorption. At this time, the chances of the formation of active species ($\mathbf{OH^{\bullet}}$ & $\mathbf{O_2^{-\bullet}}$) are very less on the surface of the catalyst. Finally, we concluded that 10 mgL^{-1} of pollutants showed the highest rate constant (5.12×10^{-3} min^{-1} for 4-NP and 7.49×10^{-3} min^{-1} for RhB). The degradation percentages are shown in Figure S2 (Supplementary Information). The optimum

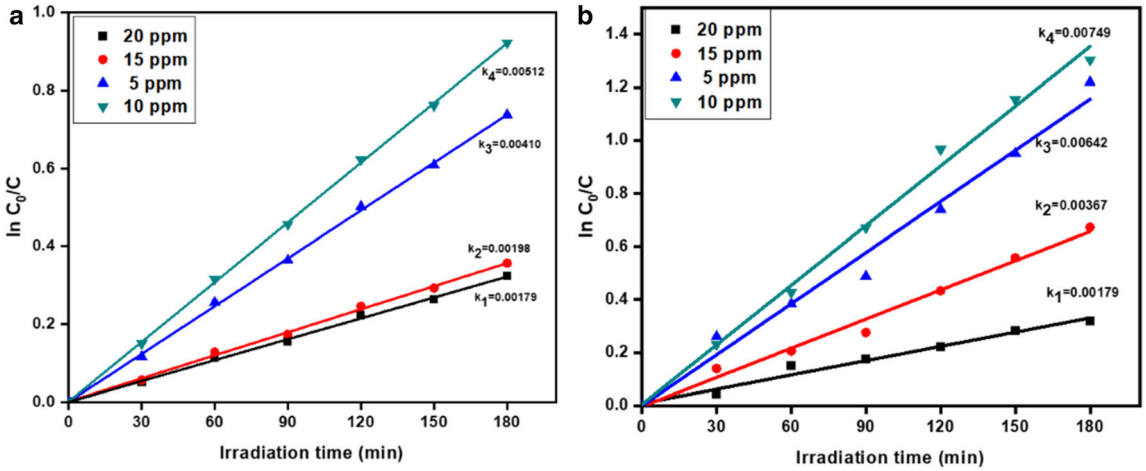

Figure 8. The kinetic plots for the pseudo-first-order reaction of the effect of concentration on 4-Nitrophenol and Rhodamine B (50 mg/50 mL, 20 ZnO/CN catalyst, 3 h irradiation time).

concentration for the removal of both pollutants is 10 mgL^{-1}.

3.6c *Effect of amount of the catalyst on 4-nitrophenol and Rhodamine B degradation*: As we know, the quantity of the catalyst also shows the impact on the mineralization and degradation of the pollutants. Herein, we varied the catalyst (20 ZnO/CN) quantity of 30 mg/50 mL to 60 mg/50 mL; in the results, the rate constant and activity of the catalyst were changed, i.e., increased due to the presence of a higher number of active sites. From Figure 9, we conclude that 50 mg/50 mL provided the highest rate constant 5.12×10^{-3} min^{-1} for 4-NP and 7.49×10^{-3} min^{-1} for RhB. The degradation profiles are shown in Figure S3 (Supplementary Information). Therefore, based on the above results, we optimized the catalyst quantity, i.e., 50 mg/50 mL.

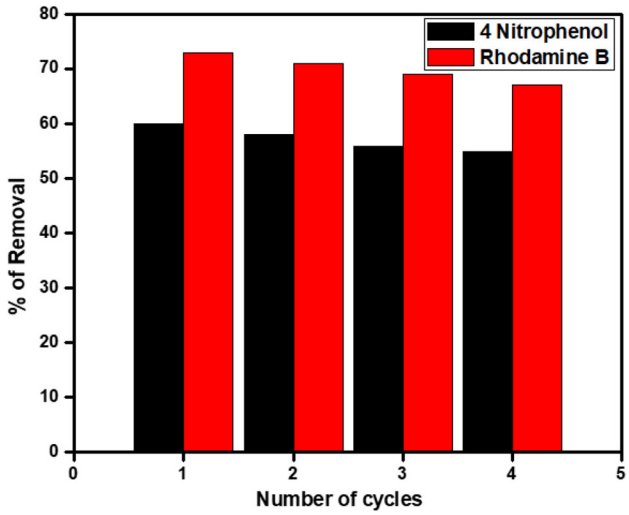

Figure 10. Reusability studies of Rhodamine B and 4-Nitrophenol.

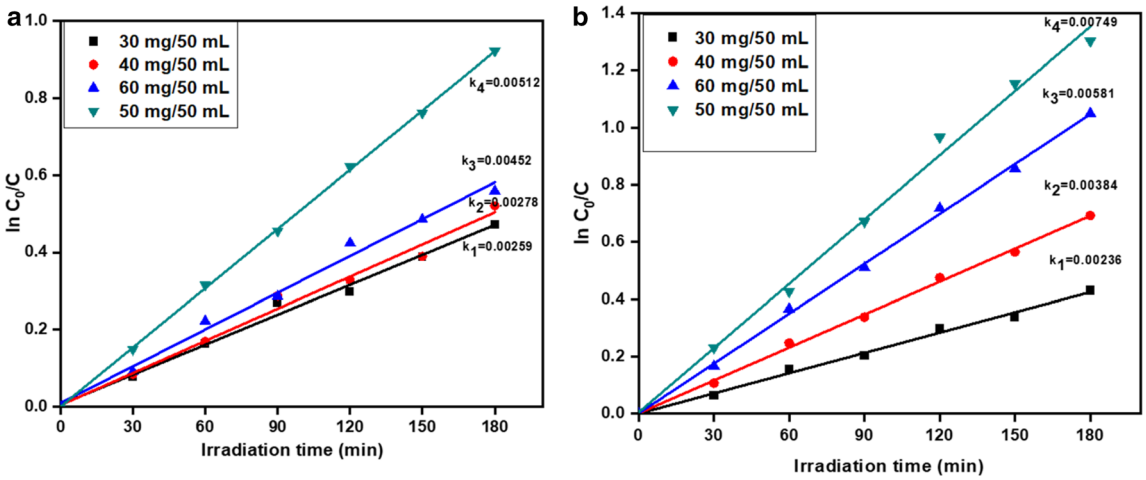

Figure 9. The kinetic plots for the pseudo-first-order reaction of the effect of a catalyst on 4-NP and Rhodamine B. (10 ppm 4 NP, 10 ppm RhB, 3 h irradiation time).

3.6d *Reusability study*: Figure 10 depicts the reusability profile of the photocatalyst. The photocatalyst 20 ZnO/CN was reused by recovering the catalyst by centrifugation and washing with water and ethanol followed by drying in a hot air oven at 80 °C overnight. The recovered catalyst was tested for the next cycles and used for removing of 4-Nitrophenol and Rhodamine B under visible light irradiation. The slight activity loss after the fourth cycle was due to losing some amount of catalyst during recovery. After using the catalyst four times, we observed 4 NP degradation decreased from 60% to 55%, and Rhodamine B degradation decreased from 73% to 67%. From the above results, it can be concluded that the catalyst is stable with minimal loss of activity up to 4 cycles.

3.6e *Scavenger tests for oxidizing species*: The different scavenger tests have been performed to investigate the radical species involved in the degradation process. The isopropyl alcohol (IPA), p-benzoquinone (p-BQ), EDTA, and DMSO are used as scavengers for hydroxyl radicals, superoxide radicals, holes, and electrons respectively. In this experiment, we have taken 1×10^{-4} mol dm^{-3} amount of IPA, p-BQ, EDTA, and DMSO with pollutants and 20 ZnO/CN catalyst. After 180 min of visible light irradiation, we observed degradation percentages of 29%, 37%, 56%, 59% for 4-NP and 32%, 40%, 71%, 68% for Rhodamine B, respectively, with IPA, p-BQ, EDTA, and DMSO compared to the absence of scavengers shown in Figure 11. The addition of EDTA and DMSO had a negligible effect on the photocatalytic activity of 20 ZnO/CN. The scavenging experiment identified hydroxyl radicals and superoxide radicals are the main oxidizing species during the degradation process.

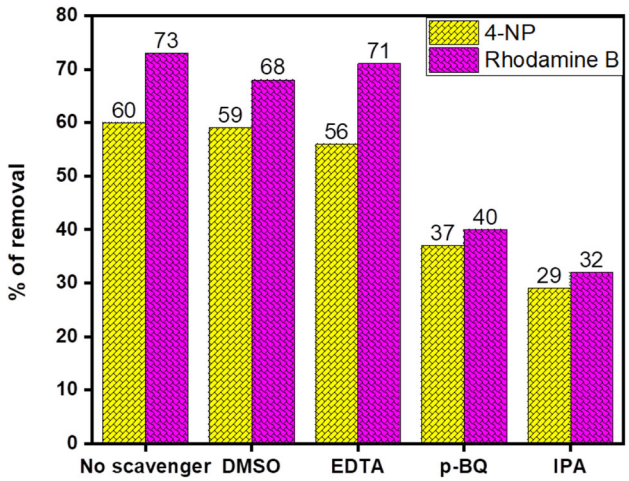

Figure 11. Effect of scavengers on photocatalytic removal of 4-Nitrophenol and Rhodamine B.

3.7 *Photocatalytic mechanism*

The mechanism involved in photocatalytic degradation of Rhodamine B and 4-Nitrophenol has been explained as follows. The conduction band and valance band edge potentials of ZnO and g-C_3N_4 are measured and a detailed discussion is shared in the supplementary information. When visible light irradiates on the ZnO/g-C_3N_4 composite, the electron-hole pairs are generated on the g-C_3N_4 side. The electrons in the conduction band (CB) of *g*-C_3N_4 are transferred to CB of ZnO (eq. 3), where atmospheric or dissolved oxygen is reduced to form superoxide radical anion ($O_2^{-}\bullet$) (eq. 4). As shown in eq. 5, the superoxide radical ion reacts with protons (H^+) to generate peroxide radical ($HOO^{\cdot}$). The peroxide radical reacts with electrons in CB of ZnO and H^+ to form hydrogen peroxide (H_2O_2) (eq. 6), which reacts with CB electron to form hydroxyl ion (OH^-) and hydroxyl radical (•OH) (eq. 7). The holes left in the VB of ZnO are transferred to g-C_3N_4(VB) (eq. 8), and these holes react with adsorbed water to form hydroxyl radical (•OH) and proton (H^+) (eq.9 and eq.10). These hydroxyl radicals (•OH) and superoxide radical anion ($O_2^{-}\bullet$) play a vital role during the degradation of Rhodamine B and 4-Nitrophenol into non-toxic products (CO_2 & H_2O).[57,58] The schematic representation of the proposed mechanism for 4-nitrophenol and Rhodamine B degradation under visible light irradiation is shown in Figure S4 (Supplementary Information).

$$e^-(CB) + ZnO(CB) \rightarrow e^-(ZnO(CB)) \quad (3)$$

$$e^-(ZnO(CB)) + O_2(atm) \rightarrow O_2^{-\cdot} \quad (4)$$

$$O_2^{-\cdot} + H^+ \rightarrow HOO^{\cdot} \quad (5)$$

$$HOO^{\cdot} + e^-(CB) + H^+ \rightarrow H_2O_2 \quad (6)$$

$$H_2O_2 + e^-(CB) \rightarrow OH^- + \cdot OH \quad (7)$$

$$h^+(ZnO(VB)) \rightarrow h^+(g\text{-}C_3N_4(VB)) \quad (8)$$

$$H_2O_{ads} + h^+(VB) \rightarrow \cdot OH + H^+ \quad (9)$$

$$h^+(g\text{ - }C_3N_4(VB)) + OH^- \rightarrow \cdot OH \quad (10)$$

4. Conclusions

In this experimental study, we successfully synthesized robust, non-toxic, and cheap ZnO, *g*-C_3N_4, and ZnO/CN catalysts. Moreover, as-prepared catalysts

were characterized by using various physicochemical techniques. Importantly, the catalyst 20 ZnO/CN showed higher photocatalytic activity (under the visible light) for the removal of 4-nitroarenes and Rhodamine B even at low concentrations. Also, we studied the effect of pollutant concentration and catalyst quantity. Specifically, kinetic study and recyclability of the catalysts are also examined.

Acknowledgements

KVA would like to thank IITH for providing fellowship. Dr. Selvaraj extends his appreciation to the Deanship of Scientific Research at King Khalid University for giving this study through the General Research Project under grant number G.R.P. 317/1442. TV is grateful to the DST-Science and Engineering Research Board (SERB) for the award of the National Post-Doctoral Fellowship (PDF/2016/003661).

References

1. Abay A K, Chen X and Kuo D H 2017 Highly efficient noble metal-free copper-nickel oxysulfide nanoparticles for catalytic reduction of 4-nitrophenol, methyl blue, and rhodamine-B organic pollutants *New J. Chem.* **41** 5628
2. Brillas E and Martínez-Huitle C A 2015 Decontamination of wastewaters containing synthetic organic dyes by electrochemical methods. An updated review *Appl. Catal. B* **166** 603
3. Subrahmanyam C, Louis B, Rainone F, Viswanathan B, Renken A and Varadarajan T K 2002 Partial oxidation of toluene by O_2 over mesoporous Cr–AlPO *Cat. Commun.* **3** 45
4. Tirado M L M, Bass M, Piatkovsky M, Ulbricht M, Herzberg M and Freger V 2016 Assessing biofouling resistance of a polyamide reverse osmosis membrane surface-modified with a zwitterionic polymer *J. Membr. Sci.* **520** 490
5. Rajasulochana P and Preethy V 2016 Comparison on the efficiency of various techniques in the treatment of waste and sewage water—A comprehensive review *Resour. Effic. Technol.* **2** 175
6. de Abreu Domingos R and da Fonseca F V 2018 Evaluation of adsorbent and ion exchange resins for removal of organic matter from petroleum refinery wastewaters aiming to increase water reuse *J. Environ. Manag.* **214** 362
7. Oncel M S, Muhcu A, Demirbas E and Kobya M 2013 A comparative study of chemical precipitation and electrocoagulation for treatment of coal acid drainage wastewater *J. Environ. Chem. Eng.* **1** 989
8. Ali I and Gupta V K 2006 Advances in water treatment by adsorption technology *Nat. Protoc.* **1** 2661
9. Kumar K A, Amanchi S R, Sreedhar B, Ghosal P and Subrahmanyam C 2017 Phenol and Cr (VI) degradation with Mn ion-doped ZnO under visible light photocatalysis *RSC Adv.* **7** 43030
10. Kumar K A, Lakshminarayana B, Vinodkumar T and Subrahmanyam C 2019 Cu-ZnO for visible-light-induced mineralization of Bisphenol-A: Impact of Cu ion doping *J. Environ. Chem. Eng.* **7** 103057
11. Kumar K A, Chandana L, Ghosal P and Subrahmanyam C H 2018 Simultaneous photocatalytic degradation of p-cresol and Cr (VI) by metal oxides supported reduced graphene oxide *Mol. Catal.* **451** 87
12. Hammad T M, Salem J K and Harrison R G 2013 Structure, optical properties and synthesis of Co-doped ZnO superstructures *Appl. Nanosci.* **3** 133
13. Xu S, Qin Y, Xu C, Wei Y, Yang R and Wang ZL 2010 Self-powered nanowire devices *Nat. Nanotechnol.* **5** 366
14. Ashar A, Iqbal M, Bhatti I A, Ahmad M Z, Qureshi K, Nisar J and Bukhari I H 2016 Synthesis, characterization and photocatalytic activity of ZnO flower and pseudo-sphere: Nonylphenol ethoxylate degradation under UV and solar irradiation *J. Alloys Compd.* **678** 126
15. Khan R, Hassan M S, Uthirakumar P, Yun J H, Khil MS and Lee I H 2015 Facile synthesis of ZnO nanoglobules and its photocatalytic activity in the degradation of methyl orange dye under UV irradiation *Mater. Lett.* **152** 163
16. Rajamanickam D and Shanthi M 2016 Photocatalytic degradation of an organic pollutant by zinc oxide–solar process *Arab. J. Chem.* **9** 1858
17. Nagaraja R, Kottam N, Girija C R and Nagabhushana B M 2012 Photocatalytic degradation of Rhodamine B dye under UV/solar light using ZnO nanopowder synthesized by solution combustion route *Powder Technol.* **215** 91
18. Zhang G, Shen X and Yang Y 2011 Facile synthesis of monodisperse porous ZnO spheres by a soluble starch-assisted method and their photocatalytic activity *J. Phys. Chem. C* **115** 7145
19. Intarasuwan K, Amornpitoksuk P, Suwanboon S and Graidist P 2017 Photocatalytic dye degradation by ZnO nanoparticles prepared from $X_2C_2O_4$ (X= H, Na and NH4) and the cytotoxicity of the treated dye solutions *Sep. Purif. Technol.* **177** 304
20. Trandafilović L V, Jovanović D J, Zhang X, Ptasińska S and Dramićanin M D 2017 Enhanced photocatalytic degradation of methylene blue and methyl orange by ZnO: Eu nanoparticles *Appl. Catal. B* **203** 740
21. Fardood S T, Ramazani A, Moradi S and Asiabi P A 2017 Green synthesis of zinc oxide nanoparticles using Arabic gum and photocatalytic degradation of direct blue 129 dye under visible light *J. Mater. Sci. Mater. Electron.* **28** 13596
22. Gnanasekaran L, Hemamalini R, Saravanan R, Ravichandran K, Gracia F, Agarwal S and Gupta V K 2017 Synthesis and characterization of metal oxides (CeO_2, CuO, NiO, Mn_3O_4, SnO_2, and ZnO) nanoparticles as photocatalysts for degradation of textile dyes *J. Photochem. Photobiol. B* **173** 43
23. Hernández-Urest D B, Vázquez A, Sanchez-Martinez D and Obregón S 2016 Performance of the polymeric g-C_3N_4 photocatalyst through the degradation of pharmaceutical pollutants under UV–vis irradiation *J. Photochem. Photobiol. B* **324** 47

24. Kumar S, Karthikeyan S and Lee A 2018 g-C_3N_4-based nanomaterials for visible-light-driven photocatalysis *Catalysis* **8** 74
25. Zhang G, Lan Z A, Lin L, Lin S and Wang X 2016 Overall water splitting by Pt/g-C_3N_4 photocatalysts without using sacrificial agents *Chem. Sci.* **7** 3062
26. Li X, Xiong J, Gao X, Huang J, Feng Z, Chen Z and Zhu Y 2019 Recent advances in 3D g-C_3N_4 composite photocatalysts for photocatalytic water splitting, degradation of pollutants and CO_2 reduction *J. Alloys Compd.* **802** 196
27. Ren H T, Jia S Y, Wu Y, Wu S H, Zhang T H and Han X 2014 Improved photochemical reactivities of Ag_2O/g-C_3N_4 in phenol degradation under UV and visible light *Ind. Eng. Chem. Res.* **53** 17645
28. Deng Y, Tang L, Zeng G, Wang J, Zhou Y, Wang J, et al. 2018 Facile fabrication of mediator-free Z-scheme photocatalyst of phosphorus-doped ultrathin graphitic carbon nitride nanosheets and bismuth vanadate composites with enhanced tetracycline degradation under visible light *J. Colloid Interface Sci.* **509** 219
29. Zheng Q, Durkin D P, Elenewski J E, Sun Y, Banek N A, Hua L, et al. 2016 Visible-light-responsive graphitic carbon nitride: rational design and photocatalytic applications for water treatment *Environ. Sci. Technol.* **50** 12938
30. Wang X J, Yang W Y, Li F T, Xue Y B, Liu R H and Hao Y J 2013 In situ microwave-assisted synthesis of porous N-TiO_2/g-C_3N_4 heterojunctions with enhanced visible-light photocatalytic properties *Ind. Eng. Chem. Res.* **52** 17140
31. Wang S, Li D, Sun C, Yang S, Guan Y and He H 2014 Synthesis and characterization of g-C_3N_4/Ag_3VO_4 composites with significantly enhanced visible-light photocatalytic activity for triphenylmethane dye degradation *Appl. Catal. B* **144** 885
32. Moreira N F, Sampaio M J, Ribeiro A R, Silva C G, Faria J L and Silva A M 2019 Metal-free g-C_3N_4 photocatalysis of organic micropollutants in urban wastewater under visible light *Appl. Catal. B* **248** 184
33. Zhang J, Zhang M, Sun R Q and Wang X 2012 A facile band alignment of polymeric carbon nitride semiconductors to construct isotype heterojunctions *Angew. Chem. Int. Ed.* **51** 10145
34. Jo W K, Lee J Y and Selvam N C S 2016 Synthesis of MoS_2 nanosheets loaded ZnO–g-C_3N_4 nanocomposites for enhanced photocatalytic applications *Chem. Eng. J.* **289** 306
35. Uma R, Ravichandran K, Sriram S and Sakthivel B 2017 Cost-effective fabrication of ZnO/g-C_3N_4 composite thin films for enhanced photocatalytic activity against three different dyes (MB, MG and RhB) *Mater. Chem. Phys.* **201** 147
36. Chidhambaram N and Ravichandran K 2017 Fabrication of ZnO/g-C_3N_4 nanocomposites for enhanced visible-light-driven photocatalytic activity *Mater. Res. Express.* **4** 075037
37. Chen Q, Hou H, Zhang D, Hu S, Min T, Liu B, et al. 2018 Enhanced visible-light-driven photocatalytic activity of hybrid ZnO/g-C_3N_4 by high-performance ball milling *J. Photochem. Photobiol. A* **350** 1
38. Liang B, Han D, Sun C, Zhang W and Qin Q 2018 Deposition of ZnO flowers on the surface of g-C_3N_4 by the solid-phase reaction *Funct. Mater. Lett.* **11** 1850020
39. Li L, Sun S Q, Wang Y X and Wang C Y 2018 Facile synthesis of ZnO/g-C_3N_4 composites with honeycomb-like structure by H_2 bubble templates and their enhanced visible-light photocatalytic performance *J. Photochem. Photobiol. A* **355** 16
40. Kumar S, Baruah A, Tonda S, Kumar B, Shanker V and Sreedhar B 2014 Cost-effective and eco-friendly synthesis of novel and stable N-doped ZnO/gC_3N_4 core-shell nanoplates with excellent visible-light responsive photocatalysis *Nanoscale* **6** 4830
41. Mani A D, Nandy S and Subrahmanyam C 2015 Synthesis of CdS/CeO_2 nanomaterials for photocatalytic H2 production and simultaneous removal of phenol and Cr (VI) *J. Environ. Chem. Eng.* **3** 2350
42. Reddy P M K, Raju B R, Karuppiah J, Reddy E L and Subrahmanyam C 2013 Degradation and mineralization of methylene blue by dielectric barrier discharge non-thermal plasma reactor *Chem. Eng. J.* **217** 41
43. Chandana L, Lakshminarayana B and Subrahmanyam C 2015 Influence of hydrogen peroxide on the simultaneous removal of Cr (VI) and methylene blue from the aqueous medium under atmospheric pressure plasma jet *J. Environ. Chem. Eng.* **3** 2760
44. Wang J, Yang Z, Gao X, Yao W, Wei W, Chen X, et al. 2017 Core-shell g-C_3N_4@ ZnO composites as photoanodes with double synergistic effects for enhanced visible-light photoelectrocatalytic activities *Appl. Catal. B* **217** 169
45. Yuan X, Zhou C, Jing Q, Tang Q, Mu Y and Du A K 2016 Facile synthesis of g-C_3N_4 nanosheets/ZnO nanocomposites with enhanced photocatalytic activity in the reduction of aqueous chromium (VI) under visible light *Nanomater* **6** 173
46. Zhang S, Su C, Ren H, Li M, Zhu L, Ge S, et al. 2019 In-situ fabrication of g-C_3N_4/ZnO nanocomposites for photocatalytic degradation of methylene blue: Synthesis procedure does matter *Nanomater* **9** 215
47. Lin X, Huang F, Xing J, Wang W and Xu F 2008 Heterojunction semiconductor SnO_2/$SrNb_2O_6$ with an enhanced photocatalytic activity: The significance of chemically bonded interface *Acta Mater.* **56** 2699
48. Vignesh K, Kang S, Kwak B S and Kang M 2015 Mesoporous ZnO nano-triangles@ graphitic-C_3N_4 nano-foils: fabrication and Recyclable photocatalytic activity *Sep. Purif. Technol.* **147** 257
49. Zhou J, Zhang M and Zhu Y 2014 Preparation of visible-light-driven gC_3N_4@ ZnO hybrid photocatalyst via mechanochemistry *Phys. Chem. Chem. Phys.* **16** 17627
50. Kong J Z, Zhai H F, Zhang W, Wang S S, Zhao XR, Li M, et al. 2017 Visible light-driven photocatalytic performance of N-doped ZnO/gC_3N_4 nanocomposites *Nanoscale Res. Lett.* **12** 526
51. Kumaresan N, Sinthiya M M A, Kumar M P, Ravichandran S, Babu R R, Sethurman K and Ramamurthi K 2020 Investigation on the g-C_3N_4 encapsulated ZnO nanorods heterojunction coupled with GO for effective photocatalytic activity under visible light irradiation *Arab. J. Chem.* **13** 2826

52. Md Rosli N I, Lam S M, Sin J C, Satoshi I and Mohamed A R 2017 Photocatalytic performance of ZnO/g-C_3N_4 for removal of phenol under simulated sunlight irradiation *J. Environ. Chem. Eng.* **5** 04017091
53. Qin H, Zuo Y, Jin J, Wang W, Xu Y, Cui L and Dang H 2019 ZnO nanorod arrays grown on g-C_3N_4 microsheets for enhanced visible-light photocatalytic H_2 evolution *RSC Adv.* **9** 24483
54. Nagaraju G, Prashanth S A, Shastri M, Yathish K V, Anupama C and Rangappa D 2017 Electrochemical heavy metal detection, photocatalytic, photoluminescence, biodiesel production and antibacterial activities of Ag–ZnO nanomaterial *Mater. Res. Bull.* **94** 54
55. Lv H, Ji G, Yang Z, Liu Y, Zhang X, Liu W and Zhang H 2015 Enhancement photocatalytic activity of the graphite-like C_3N_4 coated hollow pencil-like ZnO *J. Colloid Interface Sci.* **450** 381
56. Sun J X, Yuan Y P, Qiu L G, Jiang X, Xie A J, Shen Y H and Zhu J F 2012 Fabrication of composite photocatalyst g-C_3N_4–ZnO and enhancement of photocatalytic activity under visible light *Dalton Trans.* **41** 6756
57. Pragati F, Roshan N, Subhashis G and Barshilia H C 2015 Graphitic-carbon nitride support for the synthesis of shape-dependent ZnO and their application in a visible light photocatalyst *RSC Adv.* **5** 80397
58. Zhang B, Li M, Wang X, Zhao Y, Wang H and Song H 2018 Pompon-like structured g-C_3N_4/ZnO composites and their application in visible light photocatalysis *Res. Chem. Intermed.* **44** 6895